Advanced Symmetry Concepts and their Violation in Composite Photonic Structures

Wesleyan University

NLM DARPA Grant No HR00111820042
Final Technical Report
Performing Period: 08/06/2018-08/05/2020
Program Manager: Dr. R. Chadrasekar

PI: Dr. Tsampikos Kottos (Wesleyan University)
CoPIs: Dr. Demetri Christodoulides; Dr. Mercedeh Khajavikhan(CREOL-Univ. of Central Florida)
CoPI : Dr. Andrey Chabanov (University of Texas at San Antonio)
CoPIs:Dr. Gregory Salamo and Dr. Fisher Yu (University of Arkansas)
CoPI : Dr. Lan Yang (Washington University in St. Louis)

Report Prepared by: Dr. Tsampikos Kottos
Department of Physics, Wesleyan University
Exley Science Tower, 265 Church Street
Middletown CT-06459, USA
Tel: 860-6852036
Email: tkottos@wesleyan.edu

1. Rationale of Project, Objectives and Executive Summary of Basic Results

Background: Symmetry in nature is reflected in the laws of physics. Consequently, in optics one can expect that the manipulation of symmetries, and especially their violation, whether explicit or spontaneous, will lead to altogether new regimes for light-matter interactions. In optics, diffraction gratings, photonic crystals, and meta-materials are notable examples of such efforts where the ***geometrical*** (static) symmetries of the unit cell can shape the response of a system. A more remarkable possibility, however, is to go beyond such visibly ordered arrangements by designing structures in which the underlying symmetries are ***dynamical*** and hidden instead in the equations that dictate the dynamics of the system. Such dynamical symmetries mandate the conservation laws that the system has to obey, and hence its evolution.

In this regard, the discovery of new engineering strategies which also utilize gain, loss, and nonlinear mechanisms in order to manipulate dynamical symmetries, such as time-reversal, chiral, and spatial symmetries, could enable a breakthrough in the control of electromagnetic wave propagation and bring light-matter interaction effects to a new extreme. While these symmetries differ, they have in common that in the vicinity of a symmetry breaking point, the system develops a bifurcation (extreme response point) in some parameter space. As a result, an infinitesimal perturbation causes an "extreme response" in one or multiple branches. In the frame of photonics, a small change in a parameter near a bifurcation point can produce a huge amplification of light-matter interaction, which can have significant impact on applications. However, universal models that understand how to design optical structures characterized by these extreme response points, and quantify topological changes in their vicinity, do not exist.

Objective: We proposed to develop strategies that utilize dynamical (hidden) symmetries in order to achieve extreme light-matter interactions. The latter can be harvested in various forms: as extreme system sensitivity for hypersensitive sensing, protocol designs for robust operational efficiency against fabrication errors, giant non-reciprocal transport, or unparalleled optical limiting action against harmful incident radiation etc. During phase I we have shown that, irrespective of its specific form, this extreme response has ***always*** the same physical origin - namely the preparation of the photonic system near symmetry violation points. We have capitalized on this new idea by developing strategies which allow us to approach the symmetry violation points via all available optical degrees of freedom (space, time and phase). Using this methodology, we have advanced the state of the art of various photonic systems relevant to DoD and defense industry, including ring-laser gyroscopes with orders of magnitude *enhanced rotation sensing*, synthetic Floquet networks for non-reciprocal transport, and a new generation of *self-protective* photonic limiters.

2. Research Accomplishments

This grant supported (in total or partially) 25 publications in peer review journals, and seven conference proceedings. Below we provide the highlights of the research accomplishments, following the goals as indicated the Research Description Document (RDD). The related publication (see list of published papers) are indicated next to the subject-task line inside square brackets.

Task 1.1 Enhanced light-matter interactions at an exceptional point for rotation sensing [4,8,10,15,21,23,24].

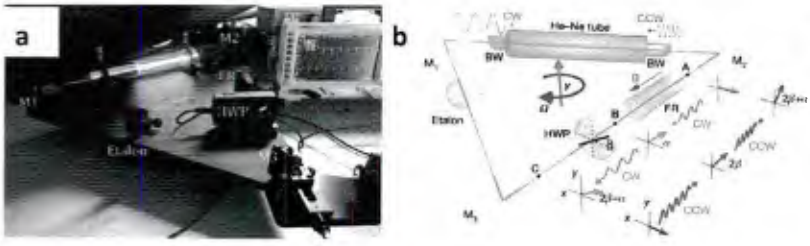

Figure 1: (a) A photograph of the He-Ne ring laser gyroscope and (b) Layout of the RLG architecture used in our experiments.

We have demonstrated for the first time a new class of non-Hermitian ring laser gyroscopes that can display an enhanced Sagnac sensitivity. Specifically, we have experimentally show that the sensitivity of a standard Helium-Neon (He-Ne) ring laser gyroscope can be significantly enhanced provided that its resonator is judiciously modified so as to support an exceptional point, see Fig. 1. As opposed to a standard RLG, the retrofitted cavity involves a Faraday rotator along with a half-wave plate (HWP). These two elements acting in conjunction with the Brewster windows (BW), incorporated on both ends of a He-Ne gain tube, were used to introduce a differential loss contrast (or gain) $\Delta\gamma$, between the clockwise (CW) and the counterclockwise (CCW) lasing modes. Finally, in order to establish an exceptional point in this cavity, it was necessary to antagonize this differential loss with a mode-coupling process. In our system, the coupling between the CW and CCW modes is readily induced using a weakly scattering object (SC), like for example an etalon. Over the course of Phase I we have achieved a 20-fold improvement in Sagnac sensitivity as compared to a standard He-Ne RLG, see Fig. 2. Finally, we have initiated a theoretical analysis for an alternative EP-RLG scheme which is based on non-reciprocal III-V active platforms. This study remained at a preliminary stage.

In parallel, we have studied the effect of noise on the sensitivity enhancement in PT-symmetric systems biased at exceptional points (EP). Specifically, the effects of thermal noise on the sensitivity of EP has been investigated by analyzing the response of a prototype PT-symmetric microwave circuit. We found that a PT-symmetric sensing scheme has the same thermal noise level compared with its Hermitian counterpart while at the same time has a dramatically improved EP sensitivity. On the quantum level, we have developed a quantum noise theory to calculate the signal-to-noise performance of an EP photonic sensor. A quantum Fisher information has been used in order to extract a lower bound for the signal-to-noise ratio (SNR) and show that parametrically improved SNR is possible for PT-symmetric systems at EP.

Finally, portion of our effort was to develop strategies that shield the EP from unwanted perturbations (e.g. fabrication errors) while retaining its high sensitivity for a specific set of perturbations. To address this problem, we introduced a new design concept which exhibits a hypersurface of Jordan EPs embedded in a larger space, and having the following peculiar features: (1) A large class of undesired perturbations shift the operating point along the exceptional surface (ES), thus, leaving the system at another EP which explains the robustness; (2) Perturbations due to back reflection or backscattering force the operating point out of the ES, leading to enhanced sensitivity.

Below we provide a detail description of the main achievements of Task 1.1 during Phase I of the project.

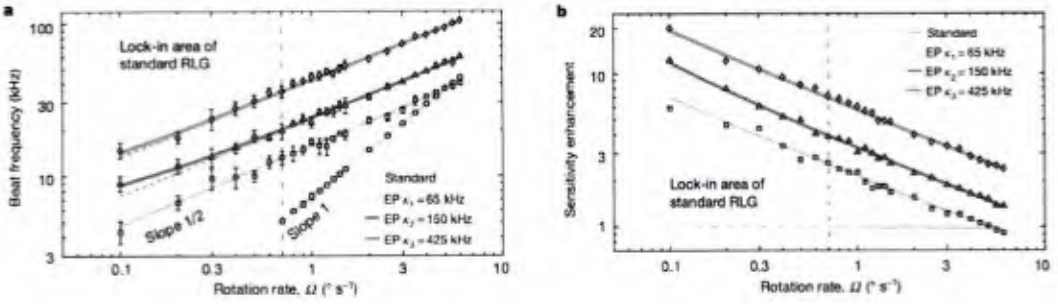

Figure 2: Enhanced Sagnac sensitivity in a He-Ne RLG system due to the presence of an exceptional point (b) Sensitivity enhancement as a function of the rotation rate.

1. Ring laser gyroscopes with enhanced Sagnac sensitivity: Gyroscopes are among invaluable elements for monitoring and maintaining the orientation and rotational velocity in airplanes, submerged submarines, space stations, telescopes and in general in any applications related to navigations. The working principle of gyroscopes is based on the Sagnac effect- a relativistically induced phase shift that scales linearly with the rotational velocity. In ring laser gyroscopes (RLG), a resonance splitting in the emission spectrum is a demonstration of this phase shift which can be detected as a beat frequency. The increased demands in modern navigation systems to more precise RLGs, has inspired research activities to enhance the sensitivity of RLGs beyond the limitations imposed by geometrical constraints. Toward this pursuit, we established a method using the enhanced sensitivity of non-Hermitian singularities or exceptional points (EPs) and experimentally reported an increase up to 20 times in the resonance splitting by working in the vicinity of EPs. The enhanced sensitivity of EP based systems is a direct byproduct of Puiseux generalized expansions and is fundamental by nature. While in Hermitian systems, the response to a perturbation ε in the best case would be of the order ε, for a Non-Hermitian system supporting an EP of order N where N eigenvalues coalesce and their corresponding eigenvectors collapse on each other, the reaction is expected to follow an Nth-root behavior ($\varepsilon^{1/N}$). Given that $\varepsilon^{1/N} \gg \varepsilon$ for $\varepsilon \ll 1$, we achieved an ultrasensitive RLGs based on these non-Hermitian spectral singularities.

To implement the RLG with an EP based enhanced Sagnac sensitivity, we used a custom-made, He–Ne RLG (purchased from Luhs; https://luhs.de/lm-0600-hene-laser-gyroscope.html). (Fig. 1a). The triangular cavity had a length of 138 cm and supported a free spectral range of about 216 MHz at 632.8 nm. It was retrofitted with an etalon which promoted lasing in a specific longitudinal mode while providing some level of coupling between clockwise (CW) and the counterclockwise (CCW) lasing modes. A terbium gallium garnet (TGG) Faraday rotator providing up to about 4° rotation at a magnetic induction of about 80 mT and a half-wave plate (HWP) with a rotation angle varying in a controlled manner with a resolution of 0.005° were introduced to the cavity which in conjunction with two Brewster windows (BW) incorporated on both ends of the He–Ne gain tube, set a differential loss contrast (or gain contrast), Δg, between the CW and CCW modes.

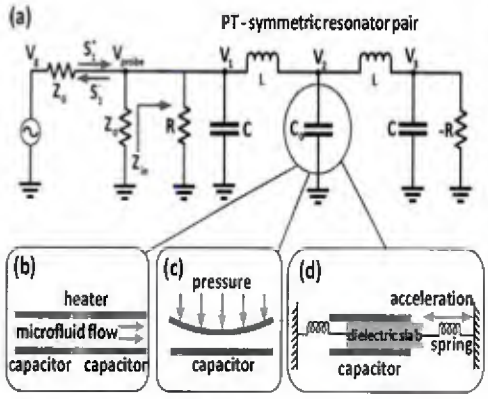

Figure 3: Hypersensitive PT-symmetric sensing circuit design and its possible application scenarios. (a) PT-symmetric sensing circuit. The pink region consists of a pair of PT-symmetric resonators. It is connected in shunt to a resistance Z_0 and then in series to a microwave generator with internal impedance Z_0. (b) Supersensitive microfluid flow sensor based on capacitive perturbation. The microfluid speed is sensed by measuring the temperature gradient created by the heater. (c) Supersensitive pressure sensor based on capacitive perturbation. A pressure sensitive membrane responds to external pressure and changes the effective capacitance of C_0. (d) Supersensitive accelerometer based on capacitive perturbation. Acceleration is sensed by attaching a dielectric slab sandwiched within the capacitor plates and connected to two springs.

To establish an EP in the cavity, this differential loss should be counteracted with a mode-coupling process. In our system, the coupling between the CW and CCW modes was induced using a weakly scattering object (for example, an etalon). The corresponding mechanism and the evolution of the state of polarization is illustrated in Fig. 1b. Once an EP was established, the Sagnac frequency splitting varied as $\sqrt{\Omega}$ as opposed to Ω, in a Hermitian cavity. Figure 2 compares the variation of the beat frequency as a function of rotation rate (Ω) for a standard RLG with our EP biased RLG working at three different coupling strengths (κ). While the response of the standard configuration is linear with respect to Ω (slope of 1), for the non-Hermitian embodiment it varies as the square-root of the rotation rate, as is evident from the slope of the corresponding Log-Log curves, which is very close to 1/2—a clear indication that an EP is at play.

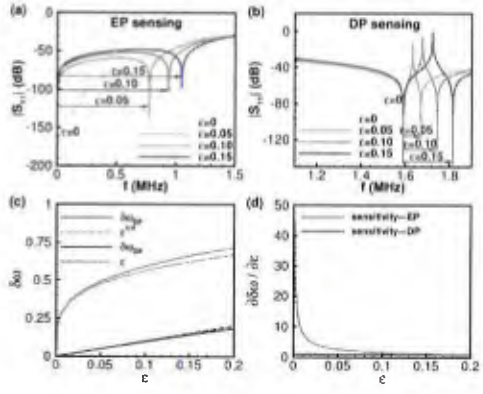

Figure 4: Amplitude of reflection coefficient, eigenfrequency shift, and sensitivity at EP and DP. (a) Amplitude of reflection coefficient with different perturbation strength for EP sensing system. (b) Amplitude of reflection coefficient for DP sensing system. (c) Eigenfrequency shift at EP and DP, dashed lines represent the corresponding series expansion truncated to the first order. (d) Sensitivity at EP and DP versus the perturbation. The components are chosen as follows: $\boldsymbol{L = 10\mu H, C = 100pF, R = 618.030\ \Omega,}$ $\boldsymbol{Z_0 = 50\ \Omega}$. For EP sensing system $\boldsymbol{C_0 = 323.6pF}$; for DP system $\boldsymbol{C_0 = 0.1\mu F}$. The above ADS simulation results confirmed our theoretical analysis.

2. Enhanced Sensing and non-degraded performance in the presence of thermal noise or/and mesoscopic fluctuations: We have also extended our investigations for EP-sensors to the design of an RF enhanced sensing scheme which is based on a sixth-order EP supported by a PT-symmetric electronic circuit [see Fig. 3]. Instead of detecting the resonant frequency splitting, we detected the eigenfrequency shift by measuring the reflected signals at the lossy side of our circuit. First, we set our system to a static EP with zero eigenfrequency. When the system is perturbed from the ideal EP condition, a reflection dip emerges, and shifts away from the static point. The reflection dip exactly matches the purely real eigenfrequency of the system under perturbation and shows a resonant shift following a fourth-order root law with respect to the perturbation strength [Fig. 4]. These resonant shifts can be measured with high resolution, even for very weak perturbations. We further verified this claim through a comparative study of our EP sensing scheme with a DP sensing protocol supported by a similar circuit layout [Fig. 4]. It turns out that our PT -symmetric RF

circuit not only serves as a sensing platform, but also filters out high-frequency thermal noise, leading to a nearly identical thermal noise level compared to the corresponding Hermitian DP sensing scheme. Considering the combined high-sensitivity, improved resolution, and nondegraded thermal noise performance, we envisioned that accelerometers, pressure sensors, or microfluid flow speed sensors (see Fig. 3) may be implemented following this scheme with unprecedented sensitivity, resolution, and excellent thermal noise performance.

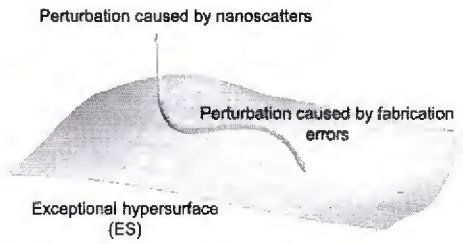

Figure 5: A non-Hermitian photonic structure can combine robustness together with sensitivity if it exhibits a hypersurface of exceptional points with the following properties: (a) Undesired perturbations due to fabrication imperfections and experimental uncertainties shift the spectrum across the surface, leaving the system at an EP. (b) Perturbations accounting for the quantities to be measured force the spectrum out of the surface i.e. away from the EPs.

We have also theoretically explored the role of mesoscopic fluctuations and noise on the spectral and temporal properties of systems of PT-symmetric-coupled gain– loss resonators operating near the EP. We have shown that an experimentally inevitable detuning in the frequencies of the uncoupled resonators might lead to an unavoidable modification of the conditions for reaching the EP, while, as this point is approached in ensembles of resonator pairs, statistical averaging significantly smears its spectral features. We analyzed how these fluctuations affect the sensitivity of sensors using as a prototype system, a set of coupled PT-symmetric resonators. The analysis shown that temporal fluctuations in the detuning and gain of these sensors lead to at least a quadratic growth of the optical power in time.

Figure 6: Schematic diagram of a proposed photonic structure that satisfies the criteria mentioned in Fig. 5. It consists of a microring resonator coupled to a waveguide that has a mirror on one side and is reflectionless at the other end. The relevant design parameters are indicated in the figure. In the absence of any reflective perturbations, the system exhibits an EP. Any variations of the coupling coefficients or the resonant frequency of the cavity will still leave the system at an EP. On the other hand, if a nanoscatterer (or any other form of reflective perturbations) comes to the vicinity of the ring, it will introduce a bidirectional coupling between the CW and CCW waves and shift the system away from the EP which, in turn, will leave a fingerprint on the emission spectrum of the system (if used in the lasing regime) or the power scattering spectrum (if operated in the amplification regime).

3. New photonic designs with enhanced robustness of EPs against fabrication imperfections: During Phase I we have also devised novel design strategies that protect EP against fabrication imperfections. Some of our theoretical schemes involved concepts from topological photonics while other involved the development of a new non-Hermitian photonic structure that exhibits an exceptional hypersurface (ES) embedded in a high-dimensional parameter space. This, in turn, provides additional degrees of freedom that can be exploited to combine robustness with enhanced sensitivity. Particularly, robustness can be achieved if the system's response is tailored such that a large class of fabrication errors and experimental uncertainties shift the operating point along the ES. On the other hand, enhanced sensitivity can arise if the perturbation due to the measurements forces the spectrum away from the ES, causing large splitting of the resonant frequency (as compared to that associated with diabolic points (DP)). This generic concept is illustrated schematically in Fig. 5 and can be implemented by a setting shown in Fig. 6. An alternative microresonator design scheme is shown in Fig. 7

demonstrating a similar type of exceptional hypersurfaces. The ES is generated by adding an appropriately designed S-bend to a ring resonator (Fig. 7b). The S-bend allows coupling between CCW (CW) to CW (CCW) modes, while prohibiting the energy exchange in the opposite direction. Such chiral elements break the rotation symmetry of the ring cavities by providing an asymmetric coupling between the clockwise (CW) and the counterclockwise (CCW) traveling modes, hence creating a hypersurface of exceptional points – as long as the coupling from one direction to the other is zero. At the EP that reside is such ES, the ring resonator becomes unidirectional (the rotation symmetry of the ring breaks), thus suppressing one of the counter-propagating modes. We have experimentally investigated the unidirectional emission in such systems below and above the exceptional point. Finally, unidirectional emission has been demonstrated in systems of two S-bend ring resonators coupled through a link structure.

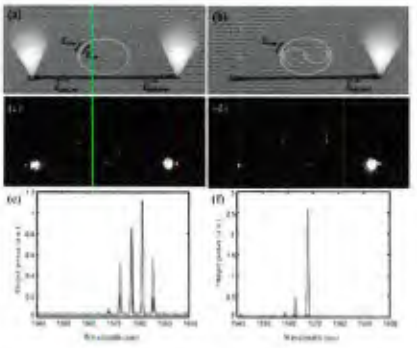

Figure 7: (Left column) Standard laser microcavity, demonstrating lasing for CW and CCW propagating modes. (Right column) A laser microcavity with an S-bend violates the rotational symmetry of the system leading to a unidirectional emission. This is a signature of an EP degeneracy.

Task 2.3 Synthetic Time-Periodic (Floquet) Networks for Non-Reciprocal Transport [3,12,13,16,19,25]

We have developed a theoretical framework that utilizes an extended Hilbert-Floquet (HF) space where a Floquet network with an extra (frequency) dimension naturally arises. The connectivity of this HF lattice dictates the Fourier harmonics of the driving signal while the coupling amplitudes between lattice sites controls the amplitudes of the respective Fourier components. The latter can be separated into real and imaginary elements describing directionless/ directed couplings in the HF lattice. Thus by judiciously engineering the directed couplings and subsequently the emerging directional paths in the HF lattice we were able to control the Fourier content of the driving signal that governs non-reciprocal optical transport. Subsequently, we have developed a formalism/modeling through which one can synthesize driving signals capable of producing non-reciprocal transport within predefined frequency windows and band-widths. The developed methodology was employing a Floquet engineering scattering theory that was utilizing the consept of effective Hamiltonians of periodically driven systems. This approach allowed us to develop a systematic high-frequency expansion of the Floquet scattering matrix, which unveiled the important role of micromotion in modifying the coupling of the system to the leads. We demonstrated the efficiency of our scheme by theoretically proposing (and computationally testing) driving protocols that can be implemented in photonic circuits for enhanced (optimized) nonreciprocal transport (NRT). Implementation of this methodology to coherent perfect absorption associated with periodically driven targets and non-reciprocal up/down frequency conversion has also been investigated and established via specific theoretical/numerical examples.

We have also expanded these Floquet-network algorithms for the control of thermal radiation in photonic circuits. In parallel, we have demonstrated that when the target is periodically modulated via an adiabatic variation of some control parameters, such that an EP singularity is enclosed in the parameter space during one period of the modulation, the scattered field is

extremely robust to the specific form of the incident wave and to interference effects generated during the scattering process via the wave-matter interaction.

Finally, during Phase I, we have developed an experimental platform where synthetic Floquet (periodically modulated) lattices, have been realized using fiber loop arrangements. Specifically, an omnipolarizer action was demonstrated by dynamically enclosing (via adiabatic modulations) an exceptional point. This goal was achieved by imposing a constant coupling strength, and temporal variations of gain (or loss) and detuning between two orthogonal polarization components. The proposed platform was implemented in a 300 m single mode fiber loop where the evolution of the polarization state of a single pulse was monitored.

Below we provide a detail description for some of our main achievements associated with Task 2.3 during Phase I of the project.

1. Floquet engineering scattering (FES) theory: We have developed a *scattering Floquet engineering* approach which is applicable in the high driving-frequency limit. The method utilizes the notion of the effective (Floquet) Hamiltonian which have been recently developed in the framework of wave-packet dynamics of Floquet systems. The approach highlights the importance of micromotion in the scattering framework and allowed us to design driving schemes with predefined transport characteristics. We have demonstrated the efficiency of our scheme in order to design a novel class of driving-induced nonreciprocal components with minimal complexity, i.e., nonreciprocal setups consisting of a minimal number of modes having the simplest connectivity (Fig. 8 left). In our analysis we have used a universal framework provided by coupled mode theory.

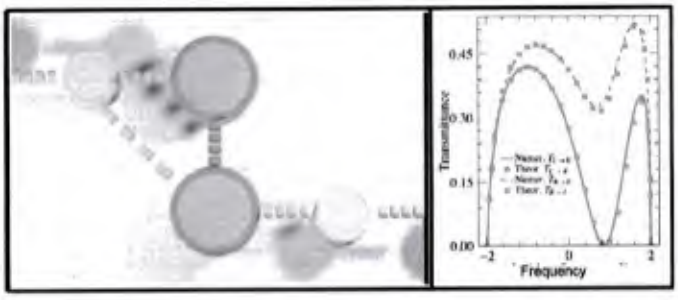

Figure 8: (Left) An optical isolator based on two-mode modulated target. In the specific case the modulated elements have been designed to be the resonant frequency of each mode and the coupling between them (Red highlights indicate the components which are modulated in time). (Right) Left/right transmittances versus the incident frequency for a driving scheme that has been indicated using the FES method as the optimal for nonreciprocal transport for the configuration of the system shown in the left subfigure.

Although the developed methodology was formally applicable at the high-modulation frequency limit, it also provided guidance for the design of nonreciprocal components in the low-frequency modulation regime. The proposed FES methodology highlights the importance of physical loops in these designs i.e., ringlike spatial configurations. Moreover, it allowed us to derive analytical expressions for the left and right transmittance asymmetry $\Delta = T_{L\to R} - T_{R\to L}$, which, in the high-frequency modulation regime, is $\Delta \sim O(\frac{1}{\omega})$. We have found that the theoretical expressions that describe the transmittance asymmetry Δ of this class of isolators and circulators matches nicely with the numerical results and, see Fig. 8 (right).

2. Control of Thermal Radiation via an Adiabatic modulations around EPs: We have expanded our Floquet-network algorithms for other applications e.g. control of thermal radiation in photonic circuits. Specifically, we have proposed a scheme that allowed us to control the direction and magnitude of thermal radiation, between two bodies at equal temperature (in thermal equilibrium),

by invoking the concept of *adiabatic pumping*. Within a resonant near-field electromagnetic heat transfer framework, we utilized an instantaneous scattering matrix approach to unveil the critical role of wave interference in radiative heat transfer. We found that appropriately designed *adiabatic* cycling near EP singularities can dramatically enhance the efficiency of the directional energy transfer. We confirmed our theoretical predictions and results that utilized a coupled mode theory framework, by performing time-domain simulations using a realistic electronic circuit set-up, see Fig. 9b.

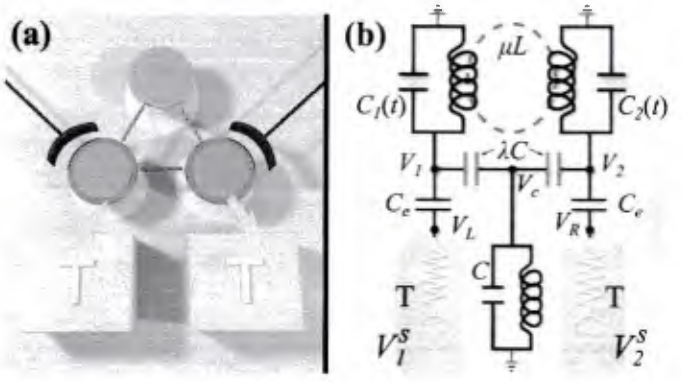

Figure 9: Proposed implementations of our thermal radiation pumping scheme: (a) A nano-photonic structure consisting of three single-mode resonators. The resonant frequencies of the first and third resonator (purple colors) are periodically modulated via a weak adiabatic modulation of the permittivities of the resonators. The system is in contact with two independent baths at the same temperature T. (b) A circuit consisting of three LC resonators. Two of these resonators are modulated via their (purple) capacitances. The circuit is coupled capacitively to two artificial reservoirs at the same temperature T. The reservoirs are implemented by synthesized noise sources generating random voltages $V_{1,2}^S$ with a prescribed spectral distribution. The positive direction for the pumped flow is chosen to match the green arrows

3. Fiber-based omni-polarizers by utilizing adiabatic modulations around EPs: At the EPs the eigenvalues and eigenvectors coalesce. Several theoretical and experimental studies have shown exciting and intriguing phenomena related to the dynamical encircling of an EP. Besides, novel devices have been proposed by using the chiral mode conversion mechanism of enclosing an EP. For instance, an on-chip polarizer with a fixed encircle loop has been numerically studied by members of our group. Robust mode conversion at the output of the waveguide was determined by the direction of encirclement regardless of the initial polarization. The closed path was tailored by imposing spatial variations of gain, and birefringence and the encirclement direction was controlled for the sense of the propagation of the coupled beam. During Phase I, the first photonics realization of an omnipolarizer action via enclosing an EP was experimentally observed. Our platform was assumed as a discrete system and was described by a non-Hermitian Hamiltonian with an EP of order two located at $(g_{EP}, \delta_{EP}) = (2\kappa, 0)$. Unlike the previously proposed omnipolarizer based in a waveguide, we introduced a versatile fiber loop system where the circular paths were used. The trajectories were tailored by carefully selecting a constant coupling strength and discrete-time variations of the gain (Gn) and detuning (δn). This experimental approach allowed us to monitor the polarization state of a pulse on the encirclement path.

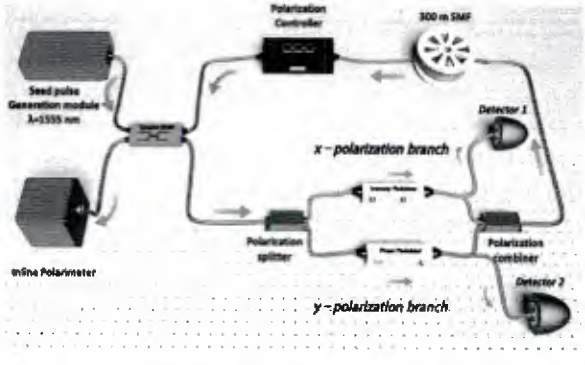

Figure 10: Schematic diagram of the proposed omnipolarizer based on fiber-loop platform

Our proposed omnipolarizer system shown in Fig. 10 was operating in the following manner: A single 100-300 ns pulse was coupled into a 300 m fiber loop comprised

by a 3 dB coupler. Then, the pulse was separated into two orthogonal polarization components: x and y. The x-component experienced gain (or loss) time modulation, while the y-component underwent temporal detuning variations. Simultaneously, the temporal signal of the detuning controlled the sense of the encirclement (clockwise or counterclockwise). In each roundtrip, the polarization components were tracked using two photodetectors. The 95% remaining of the polarization components were coupled back together. The coupling strength between both polarization components was introduced by using an electrically driven polarization controller. After that, half of the energy of this single pulse was decoupled of the omnipolarizer, and the polarization evolution per roundtrip was monitored by using an inline polarimeter and a photodetector. The remaining of the pulse went back to recirculate into the fiber system, and according to our numerical analysis, the pulse completes a cycle around the EP after 300 roundtrips along the fiber loop.

Figure 11a shows the numerical analysis of the omnipolarizer without any discrete-time modulation of gain (or loss) and birefringence. Here, we demonstrated that the non-Hermitian Hamiltonian of the system is conservative when Stokes parameter S2 is constant. In Fig. 11b we experimentally observed that the Stokes parameter S2 condition was satisfied without imposing temporal variations of gain (or loss) and detuning. Finally, in Fig. 11c omnipolarizer action was observed for discrete-time variations of the gain (loss) and detuning and enclosing the EP in a counterclockwise manner.

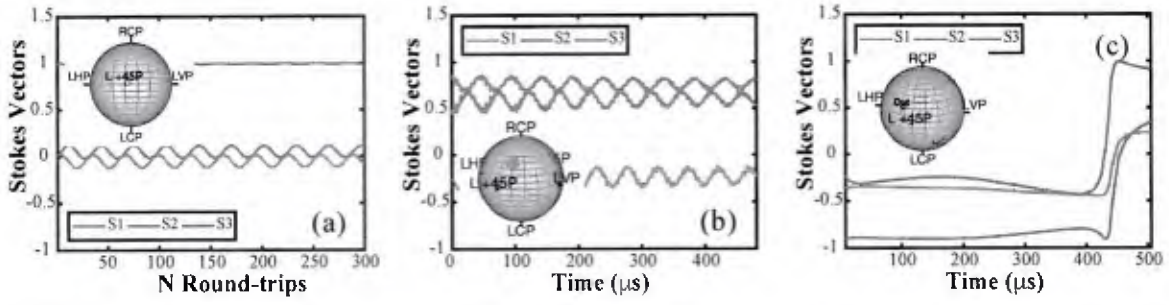

Figure 11: (a) Numerical, and (b) Experimental studies of the proposed omnipolarizer platform without use discrete time variations of gain (or loss) and birefringence. (c) Experimentally observed counterclockwise omnipolarizer action. Inset: Results shown on the Poincare sphere.

Task 3.1 Reflective Photonic Limiters [2,5,14,17,22]

Ideal optical limiters (OLs) are expected to have high transmittance at low-intensity input levels, while they block high intensity light. The transition point between low and high-intensity input is known as the limiting threshold (LT). At a certain point, the input power becomes too high even for the limiter to withstand. The respective critical point is referred to as the OL damage threshold (OLDT). The ratio between the OLDT and the LT is referred to as the limiter dynamic range (LDR). Typical OLs utilize a nonlinear optical material which is transparent at low intensities, while turning opaque (absorbing) if the light intensity exceeds the LT. This can cause overheating and destruction. In typical OL systems, nonlinear effects are used to shift the resonant frequency. Such OL cannot, however, provide broad band protection. During Phase I, we have analyzed and experimentally realized a new class of reflective photonic limiters (RPL) which: *(i)* have abrupt LT; *(ii)* are protected by the excess incident radiation by reflecting it (not absorbing it!) back to

space thus demonstrating large OLDT; (iii) provide broadband protection; (iv) are supporting high transmittance for low intensity input levels.

Two designs have been predominantly investigated theoretically, fabricated and experimentally tested successfully: (a) An Al/As/Ga/As mirror-based OL with an embedded defect InAs-based cavity that contains quantum wells. The target wavelength of this OL was in the 1-2 μm wavelength range; and (b) a cavity involving a phase-change material (VO2 in our case). The operational frequency of this second design was in the 95GHz range. In parallel, we have also theoretically proposed and experimentally test a variant of the OLs that are utilized in waveguide environment and can be used as receiver protectors in STAR systems. These receiver protectors (RP) are utilizing concepts from topological photonics in order to ensure operational robustness against fabrication imperfections. Specifically, they are consisting from a CROW array in an SSH configuration with one of the resonators coupled inductively to a diode. The theoretical study was supplemented with an experimental implementation of such design at 6.5GHz.

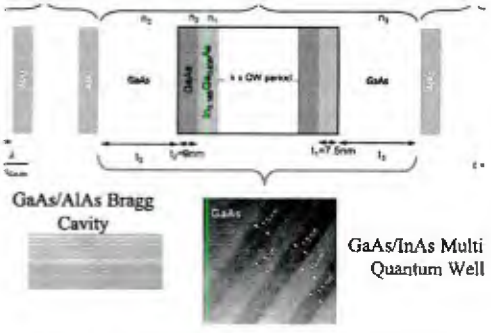

re 12: (up) A schematics of our reflective photoi
er design. (down) SEM images of the cavity and
W structure

Below we provide a detail description of the main achievements of Task 3.1 during Phase I of the project.

1. Reflective Photonic Limiters (RPL) at 1-2 μm wavelength range: The operational principle of the proposed RPL is based on the use of a defect layer with intensity-dependent (i.e. two-photon absorption) nonlinear loss tangent embedded in a low-loss multilayer periodic structure. The defect layer of the photonic structure supports a resonant defect mode whose frequency is located in the middle of the band-gap created by the multilayer structure. The low-energy pulses with central frequency close to that of the localized defect mode will pass through. But if the intensity of the pulse exceeds certain level, the entire photonic structure becomes highly reflective (not absorptive) within a broad frequency range (the band-gap). The underlying physical mechanism is based on self-regulated impedance mismatch due to the nonlinear losses which increases dramatically with the intensity of the pulse at the position of the defect layer.

QWs and 5 period Bragg mirrors. (b) Transmission as a function of intensity limits at 40% and does not saturate. (c) Low intensity transmission spectra for a RPL consisting of 20 of MQWs and period of 6 Bragg mirrors. (d) Transmission determined by z-scan limits at 30% and does not saturate. We will use a tighter focus to increase performance. The sample thickness is well within the confocal bean parameter. Transmission is corrected for substrate and wavelength filtering of the laser bandwidth by the cavity.

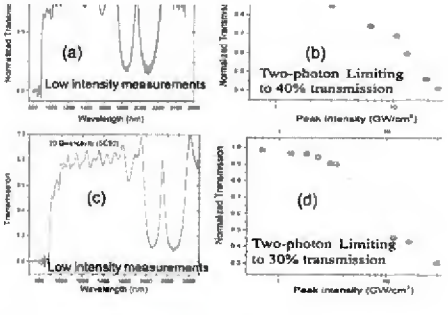

To this end we fabricated the defect cavity and high-quality Bragg mirrors based on alternating layers of (low loss) AlGaAs/GaAs semiconductor media using our team's growth facility. The defect cavity itself consisted of InAs exhibiting low linear and strong two-photon non-linear losses (see Fig. 12). Characterization of the properties of the optical material was performed and the measurements were used as inputs in the numerical modeling. The efficiency of the proposed RPL was evaluated by comparing the LDR, as extracted by our simulations, with the LDR of existing limiters. Two cavities have been designed, fabricated and tested. The first one involved 4QWs and a cavity which was formed by 5 period AlAs/GaAs Bragg mirrors and ½ wavelength cavity length. The second RPL was involving 20QWs and a cavity that was formed by 6 period AlAs/GaAs Bragg mirrors and 1 wavelength cavity length.

The Optical Limiter performance is shown in Fig. 13. In Figs. 13a we show our low intensity measurements for the transmission of a reflective photonic limiter consisting of 4 QWs and 5 period Bragg mirrors. A transmission pick ($T \approx 0.85$) occurs in the middle of the band gap at 1955nm. In (b), we report our measurements for the transmission as a function of intensity of the incident pulse. The measurements indicate a transmittance drop up to 40% and they do not show any sign of saturation for the used input peak intensities. In (c) we also report the low intensity transmittance spectra for a limiter consisting of 20 of MQWs and period of 6 Bragg mirrors. Again, a nice resonant pick around the defect mode freqeuncy is observed. Meanwhile, in Fig. 13(d), the transmission as a function of the peak intensity of the incident beam drops further down to 30% --still without any showing any signature of saturation. We point out that a tighter focus can be potentially used to increase performance. The sample thickness is well within the

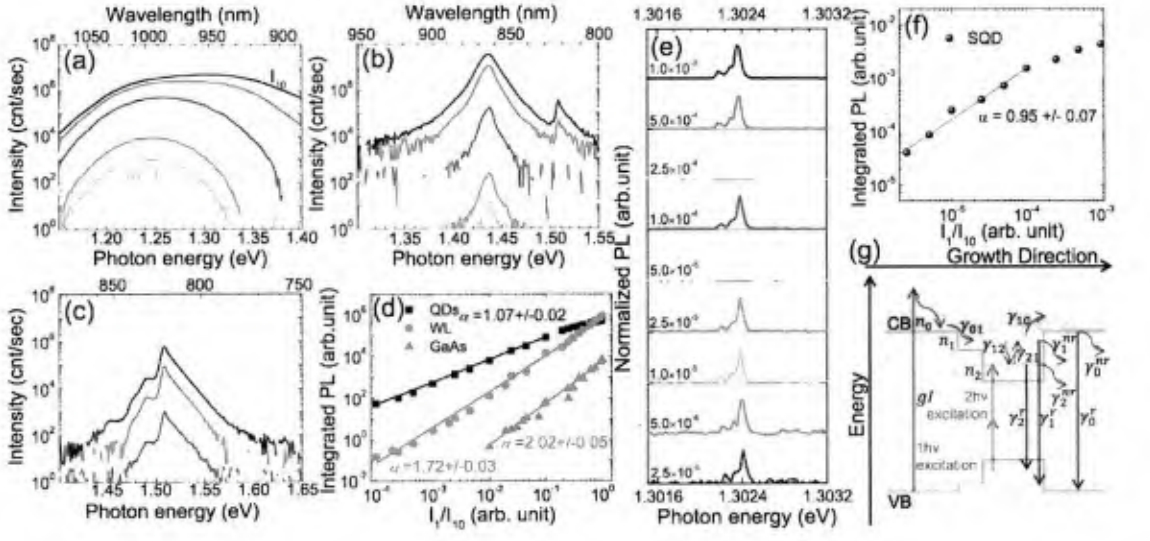

Fig. 14: 1 hν excitation power-dependent PL spectra. PL spectra at 77 K: (**a**) QD ensemble; (**b**) "WL only" sample; (**c**) GaAs wafer. The excitation power was varied from 10^{-4} I_{10} to I_{10} as labeled in (**a**). (**d**) Integrated PL intensity vs normalized 1 hν excitation power for the data in (**a**)–(**c**). The straight lines are best fits to the data with a function of $IPL = bI\alpha$, where b and α are fitting parameters. PL spectra of single QDs at 5 K: (**e**) Power dependent SQD spectra showing the ground state excitonic emissions. The numbers indicate the power ratio between the excitation power and the maximum laser power which equals to an $I_{10} \sim 6$ mW. The PL spectra were normalized to the corresponding peak intensities at 1.3024 eV. (**f**) Integrated PL intensity vs. excitation power ratio. (**g**) Schematic diagram for the three-level rate equation model. Straight arrows denote optical transitions while curve arrows denote relaxation or capture processes.

confocal bean parameter. In these measurements, the transmission is corrected for substrate and wavelength filtering of the laser bandwidth by the cavity.

We also initiated a systematic photoluminescence intensity study of MBE grown self-assembled InAs/GaAs QDs to understand its role in the optical limiter. Power dependent PL measurements were performed on ensembles of and single InAs/GaAs QDs by using one-photon (1 hv) and two-photon (2 hv) excitations. A quadratic power-law dependence of PL intensity was found on an ensemble of QDs with 2 hv excitation, which provided clear evidence for the occurrence of direct TPA in the QDs. To clarify the TPA channels, photoluminescence excitation (PLE) measurements were also conducted. A prominent peak corresponding to the ground state of the QDs was revealed in the PLE spectrum, which further confirmed the occurrence of direct TPA in the QDs. To the best of our knowledge, direct TPA in InAs QDs with excitation near its half band-gap has not been reported before. Thus, our work helps fill this gap and provides valuable insight into the direct TPA process that occurs on the versatile InAs/GaAs QDs platform for high intensity light excitations. These results are reported in Fig. 14 above.

2. Reflective Photonic Limiters using phase-change materials: We have theoretically analyzed and computationally modeled light propagation in multilayer systems with a defect cavity consisting of a phase-change-material (PCM). For the computational modeling we had used COMSOL Multiphysics software that takes into consideration electromagnetic Maxwell;s equations coupled together with a heat transfer equation. Utilizing this modeling we were able to design an optimal PCM cavity for limiting action in the W – band (75-110 GHz). As in the previous design, the PCM-based RPL involved a photonic bandgap structure, such as a multilayer cavity, incorporating the phase-change material (PCM). At low incident irradiance, the transmittance of the photonic structure is at its maximum due to resonant transmission via the localized mode that is supported by the defect cavity and has a resonant frequency inside the photonic bandgap. The high intensity radiation, however, forces the phase transition to be induced, producing an impedance mismatch which leads to an (almost) perfect reflection of the incident radiation. This high reflectivity prevents the limiter from overheating, thereby greatly increasing the limiter damage threshold.

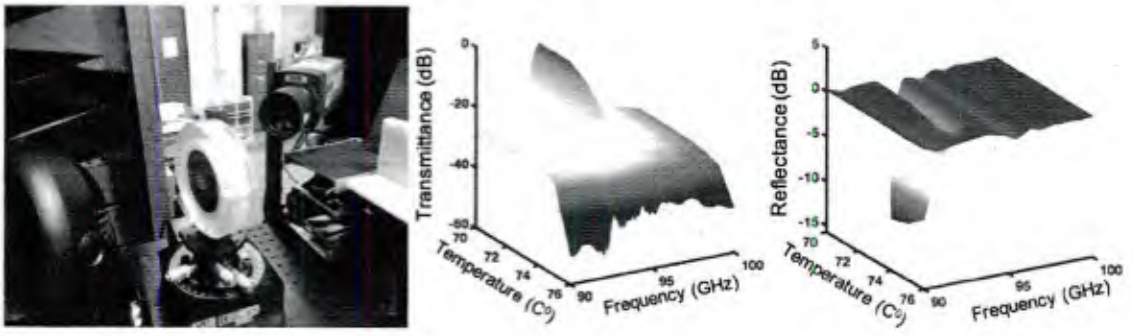

Figure 15: (left) The experimental set up associated with the W-band Reflective Optical limiter (seen in the middle of the figure, right in this figure is a an thermal camera, left in this figure is the W-band source.). The limiter is made by a photonic crystal consisting of bilayers of quarter-wavelength sapphire layers separated by air-gaps. A half-wavelength sapphire cavity incorporating a 200 nm VO2 layer is placed in the middle of the photonic crystal. The position of the VO2 is such that it coexists with an anti-nodal point of a resonant defect mode at 95GHz. The photonic crystal consists of two sapphire-spacer bilayers on the left and right of the cavity. (middle) Transmittance versus the temperature at the VO2 layer, versus frequency. When the fluence of the incident signal (CW with Gaussian profile) is such that the self-induced temperature reached ~70 Celsius, the structure undergoes an abrupt transition from an on-state (where transmittance is approximately unity) to an off-state where reflectance is now approximately unity. (right) The same as in the middle figure but now for the reflectance.

Other important advantages of the photonic design include orders-of-magnitude larger extinction ratio (the ratio of transmittances below and above the limiting threshold) and the possibility to significantly lower the limiting threshold by adjusting the photonic structure hosting the PCM. The above approach thus provides advanced broadband protection from high-level input radiation, although low intensity transmission is essentially narrowband due to its resonant nature.

Our theoretical/computational design has been tested against an experimental realization which allowed us to provide a proof of principle experimental demonstration in the W-band of a Reflective Photonic Limiters using a VO2 PCM cavity, see Fig. 15a. The photonic bandgap structure was constructed of 76.2-mm diam. c-cut sapphire (Al_2O_3) wafers, with a 525-μm thick wafer in the middle and four 256- μm thick wafers on the sides, separated by air gaps of a uniform thickness of about 792 μm. The (ordinary) electric permittivity of sapphire, was found from measurements of the insertion loss and phase of sapphire wafer in the W band, and was unchanged on heating from room temperature to 110°C. The middle sapphire wafer has been coated on one side with a polycrystalline VO_2 to a thickness of approximately 150 nm. Vanadium dioxide (VO2), undergoes an insulator-to-metal transition at a critical temperature θ_C close to 68◦C.

The VO2 limiter has been shown to function as an incident power–controlled mm-wave reflector, with a positive and negative feedback of the VO2 layer on the limiter absorptance. At low in- put power, the limiter is capable of dissipating absorbed power at a temperature below θc, so that the VO2 layer is in the dielectric phase and the multilayer structure displays a resonant transmittance at the frequency of the localized mode, see Fig. 15b. As the incident power increases, and once the absorption–dissipation equilibrium has been disturbed, the temperature of the VO2 layer quickly runs up to θ_c, due to an increase in the limiter absorptance with the increasing temperature (positive feedback). Further temperature increase, however, is counteracted by a steep drop in the absorbed power, due to the VO2 transitioning into the metallic phase and thus sharply increasing reflectance (negative feedback), see Fig. 15c. For a given high-level input power, a new equilibrium sets in at a VO2 temperature in the transition temperature interval. Thus, above the limiting threshold, the limiter is capable of safely dissipating a small and constant amount of power while reflecting most of the incident power many orders of magnitude larger, without damage to the limiter itself, see Fig. 15c. When the large input power is no longer present, the VO2 temperature drops below θc, and the limiter reverts from the high reflectivity to the resonant transmittance after a brief delay. The limiter performance, including operating frequency and bandwidth, limiting and damage threshold, extinction ratio, and on/off switching time, are determined by the design and physical properties of the limiter, ambient conditions, as well as temporal and spatial characteristics of the inci- dent radiation. In particular, in the case of a continuous wave (CW) Gaussian beam above the limiting threshold, the output power from the limiter is shown to be independent of the input power, due to a non-uniform mm-wave heating of the VO2 layer.

3. Other research directions that utilized EPs formed due to spatio-temporal symmetries [7]

During Phase I, we also studied symmetry and its violation at exceptional points in a resonator system. Through judiciously control of the coupling coefficients, gain-loss balance, and scattering in a high-quality resonator or coupled resonator systems, we could control the symmetry of the physical system and explore unconventional phenomena rising from the violation of symmetry in the system. Recent progress in non-Hermitian optics especially the exceptional points (EPs) brings about exotic optical behavior enabling the manipulation of optical states with broken symmetry.

For example, EPs have been found to enable discrete optical eigenstates with ± 1 chirality in whispering gallery mode (WGM) microresonators. We theoretically and experimentally studied transparency and absorption induced by chiral optical eigenstates at EPs in a system composed of indirectly coupled WGM resonators. By tuning one resonator to an EP, transparency or absorption occurs depending on which chirality (1 or -1) the eigenstate possesses. Based on this new physical phenomenon, electromagnetically induced transparency (EIT) can be controlled by exploiting the discrete optical eigenstates of the resonators as a control bit. Such a control method for EIT based on non-Hermitian eigenstates and chirality rather than continuous parameter tuning brings about a new opportunity for robust storing and retrieving information in optical quantum memories. More importantly, this method is compatible with the idea of state control adopted in quantum gate operation. The similar control mechanism bridges quantum computing and quantum storage which are originally two very different territories. We also studied the fundamental limits of the sensitivity of a high-Q microresonator operated around EPs. The discoveries in this project will lay the groundwork for us to design new optical sensors with superior sensitivity.

4. Technology Transfer and Collaboration with DoD Labs

An offspring of this effort was the founding of a tech company (in collaboration with industry partners) from our team-member Prof. Lan Yang. The company *DeepSight Technology Inc.* (https://deepsightinc.com/) has as a mission to transform medical diagnostics, by providing a safe and radiation-free sensing technology that can lead to a faster, cheaper and better healthcare technology. Specifically, the sensor-related concepts that have been incubated during the course of Phase I of the project have been the intellectual seeds for the formation of this company.

At the same time, Prof. Christodoulides and Prof. Khajavikhan have been partnered with Infinera in developing an on-chip EP-based RLG.

Prof. Chabanov and Prof. Kottos have been developed strong collaboration with the AFRL (Wright-Patterson and Kirkland) for the development of the PCM-based prototype reflective photonic limiter (see previous section).

5. Summary of Results and Comparison of Actual Accomplishments with the goals and Objectives of the Award

Expected Goals / Deliverables	Develop strategies to exp. Implement EP-based RLGs	Theoretically analyze and experimentally implement ring arrangement with EPs due to chiral S-bend elements	Noise analysis and fundamental limits of the EP sensitivity
Task 1.1 **Phase I**	Develop theoretical analysis, design and investigate limitations of efficiency of EP sensitivity; Exceed expectations: Proof of principle exp. demonstration of an EP-based RLG	Perform theoretical analysis and experimental realization of ring arrangements that incorporate an S-bend element. Theoretical analysis and experimental demonstration of EP degeneracies due to the presence of the S-bend	Theoretical analysis for: (a) mesoscopic noise; (b) thermal noise; (c) and development of quantum noise theory for SNR near EP

Expected Goals / Deliverables		
	Develop a formalism that allows to tailor an extended HF space via predefined driving content. Develop a Floquet engineering scattering formalism based on effective Hamiltonian formalism that allows to realize optimal non-reciprocal elements (e.g. isolators, circulators)	Experimental platform where synthetic Floquet lattices can be realized and can be utilized for non-reciprocal transport
Task 2.3 **Phase I**	A Floquet scattering formalism based on Floquet engineering methods (effective Hamiltonian formalism) has been developed and implemented for the design of efficient non-reciprocal elements (isolators, circulators).	Theor. analysis and exp. implementation of omnidirectional polarizers based on modulated fiber optics. Demonstration of state-flip effect (omnidirectional polarization) for adiabatic driving schemes around EPs

Expected Goals / Deliverables		
	Theoretical analysis, numerical modeling and design of Reflective Photonic Limiter (RPL) in the $1-2\mu m$ wavelength range	Theoretical analysis and computational modeling of RPL using phase-change materials (PCM)
Task 3.1 **Phase I**	A theoretical design and computational analysis of the performance of a RPL in $2\mu m$ range has been done. The Bragg mirror of the RPL was assumed to consist of Al/Ga/As/GaAs layer media. The defect cavity consisted of InAs with MQW exhibiting low linear and strong two-photon non-linear losses. Exceed expectation: Fabricated and tested the proposed RPL	Perform a theoretical analysis and develop numerical models using Multiphysics computational schemes that couple Maxwell's equations with heat transfer equation and describe a RPL with a PCM defect cavity. Exceed expectation: Fabricated and characterized the performance of the proposed PCM-based limiter.

6. Products, Publications, Patents, License Agreements, etc.

Publications in Refereed Journals

1) Nanolaser-based emulators of spin Hamiltonians, M. Parto, W. E. Hayenga, A. Marandi, et al., Nanophotonics 9, 419 (2020)
2) Photoluminescence of InAs/GaAs quantum dots under direct two-photon excitation, X. Hu, Xian; Y. Zhang, D. Guzun, et al., Scientific Reports 10, 10930 (2020)
3) Enhanced modulation characteristics in broken symmetric coupled microring lasers, C. Xu, W. E. Hayenga, H. Hodaei, et al., Opt. Express 28, 19608 (2020)
4) Symmetry-controlled edge states in the type-II phase of Dirac photonic lattices, G. G. Pyrialakos, N. Schmitt, N. S. Nye et al., Nat. Comm 11, 2074 (2020)
5) Self-Shielded Topological Receiver Protectors, M. Reisner, D. H. Jeon, C. Schindler, H. Schomerus, F. Mortessagne, U. Kuhl, T. Kottos, Phys. Rev. Applied 13, 034067 (2020)
6) Realizing spin Hamiltonians in nanoscale active photonic lattices, M. Parto, W. Hayenga, A. Marandi, et al., Nature Materials 19, 725 (2020)
7) Electromagnetically induced transparency at a chiral exceptional point, C. Wang, X. Jiang, G. Zhao, Guangming et al., Nature Phys. 16, 334 (2020)
8) Enhanced Sensing and Nondegraded Thermal Noise Performance Based on PT-Symmetric Electronic Circuits with a Sixth-Order Exceptional Point, Z. Xiao, H. Li, T. Kottos, A. Alu, Phys. Rev. Lett. 123, 213901 (2019)
9) 2D Solitons in PT-Symmetric Photonic Lattices, A. L. M. Muniz, M. Wimmer, A. Bisianov, et al., Phys. Rev. Lett. 123, 253903 (2019)
10) Non-Hermitian ring laser gyroscopes with enhanced Sagnac sensitivity, M. P. Hokmabadi, A. Schumer, D. N. Christodoulides, et al., Nature 576, (2019)
11) Bosonic discrete supersymmetry for quasi-two-dimensional optical arrays, Q. Zhong, S. Nelson, M. Khajavikhan, et al., Photonics Research 7, 1240 (2019)
12) Adiabatic Thermal Radiation Pumps for Thermal Photonics, H. Li, L. J. Fernandez-Alcazar, F. Ellis, et al., Phys. Rev. Lett. 123, 165901 (2019)
13) Direct Generation of Tunable Orbital Angular Momentum Beams in Microring Lasers with Broadband Exceptional Points, W. E. Hayenga, M. Parto, J. Ren, et al., ACS Photonics 6, 1895 (2019)
14) Light-induced optical switching in an asymmetric metal-dielectric microcavity with phase-change material, R. Thomas, A. A. Chabanov, I. Vitebskiy, T. Kottos, Europhys. Lett. 126, 64003 (2019)
15) Sensing with Exceptional Surfaces in Order to Combine Sensitivity with Robustness, Q. Zhong, J. Ren, M. Khajavikhan et al., Phys. Rev. Lett. 122, 153902 (2019)
16) Design Algorithms of Driving-Induced Nonreciprocal Components, H. Li, T. Kottos, Phys. Rev. Applied 11, 034017 (2019)
17) Nonreciprocity in Photonic Structures with Phase-Change Components, N. Antonellis, R. Thomas, M. A. Kats, et al., Phys. Rev. Applied 11, 024046 (2019)
18) Supersymmetric laser arrays, M. P. Hokmabadi, N. S. Nye, R. El-Ganainy, et al., Science 363, 263 (2019)
19) Dynamically modulated perfect absorbers, S. Suwunnarat, D. Halpern, H. Li, et al., Phys. Rev. A 99, 013834 (2019)
20) Observation of twist-induced geometric phases and inhibition of optical tunneling via Aharonov-Bohm effects, M. Parto, H. Lopez-Aviles, J. E. Antonio-Lopez et al., Science Advances 5, eaau8135 (2019)

21) Winding around non-Hermitian singularities, Q. Zhong, M. Khajavikhan, D. N. Christodoulides, et al., Nature Communications 9, 4808 (2018)
22) Unidirectional photonic circuit with a phase-change Fano resonator, R. Thomas, E. Makri, T. Kottos et al., Phys. Rev. A 98, 053806 (2018)
23) Fluctuations and noise-limited sensing near the exceptional point of parity-time-symmetric resonator systems, N. Mortensen, G. Asger, P. A. D. Goncalves, M. Khajavikhan et al., Optica 5, 1342 (2018)
24) Unidirectional light emission in PT-symmetric microring lasers, J. Ren, Y. G. N. Liu, M. Parto et al., Optics Express 26, 27153 (2018)
25) Floquet scattering theory based on effective Hamiltonians of driven systems, H. Li, B. Shapiro, T. Kottos, Phys. Rev. B 98, 121101 (2018)

Publications in Conference Proceedings

1) Electrically Pumped Microring Parity-Time-Symmetric Lasers, W. E. Hayenga, H. Garcia-Gracia, E. S. Cristobal et al., PROCEEDINGS OF THE IEEE 108, 827 (2020)
2) Microwave Limiters Implemented by Coupled Dielectric Resonators Based on a Topological Defect Mode and CT-Symmetry Breaking, M. Reisner, F. Mortessagne, E. Makri et al., 9th Workshop on Quantum Chaos and Localisation Phenomena Location: Warsaw, POLAND ACTA PHYSICA POLONICA A 136, 790 (2019)
3) Tunable Orbital Angular Momentum Microring Lasers Using Chiral Exceptional Points, W. E. Hayenga, J. Ren, M. Parto et al, 2019 CONFERENCE ON LASERS AND ELECTRO-OPTICS (CLEO) Book Series: Conference on Lasers and Electro-Optics (2019)
4) Supersymmetric Laser Arrays, P. M. Hokmabadi, N. S. Nye, R. El-Ganainy, et al., 2019 CONFERENCE ON LASERS AND ELECTRO-OPTICS (CLEO) Book Series: Conference on Lasers and Electro-Optics (2019)
5) Bimodal Directional Laser via Dynamically Encircling an Exceptional Point, J. Leshin, Y. Alahmadi, A. Ul-Hassan, et al., 2019 CONFERENCE ON LASERS AND ELECTRO-OPTICS (CLEO) Book Series: Conference on Lasers and Electro-Optics (2019)
6) Towards a Non-magnetic Topological Haldane Laser, Y. G. N. Liu, P. Jung, M. Parto, et al. 2019 CONFERENCE ON LASERS AND ELECTRO-OPTICS (CLEO) Book Series: Conference on Lasers and Electro-Optics (2019)
7) Mode-Dependent Coupling and Vectorial Optical Vortices in Metallic Nanolaser Arrays M. Parto, W. Hayenga, D. N. Christodoulides, et al., 2019 CONFERENCE ON LASERS AND ELECTRO-OPTICS (CLEO) Book Series: Conference on Lasers and Electro-Optics (2019)